Low-noise Double-sided Silicon Strip Detector for Soft Gamma-ray Compton Camera

Yasushi Fukazawa[a], Tatsuya Nakamoto[a], Naoyuki Sawamoto[a], Shingo Uno[a], Takashi Ohsugi[a], Hiroyasu Tajima[b], Tadayuki Takahashi[c], Takefumi Mitani[c], Takaaki Tanaka[c], and Kazuhiro Nakazawa[c]

[a]Department of Physical Sciences, Hiroshima University, 1-3-1 Kagamiyama, Higashi-Hiroshima, Hiroshima 739-8526, Japan;
[b]Stanford Linear Accelerator Center, Menlo Park, CA, USA;
[c]Institute of Space and Astronautical Science (ISAS), Aerospace Exploration Agency (JAXA), Sagamihara, Kanagawa 229-8510, Japan

ABSTRACT

A Semiconductor Multiple-Compton Telescope (SMCT) is expected to proceed a high-sensitivity soft gamma-ray observation in the energy range of 0.1–20 MeV. Double-sided silicon strip detector (DSSD) is one of key technologies for constructing SMCT, as well as the high-stopping semiconductor CdTe, because of its high energy resolution and high scattering efficiency. We have developed a low-noise system of DSSD and frontend LSI for SMCT, by optimizing geometrical structures of DSSD. We have thus obtained an energy resolution of 1.3 keV (FWHM) for 60 keV and 122 keV at -10°C in the multi-channel reading. Gamma-ray responses such as image flatness and charge splittings were found to be not problematic. We also demonstrated that our system achieved the good angular resolution close to the Doppler-broadening limit in the Compton imaging by two DSSDs.

Keywords: gamma-ray, Compton Imaging, Silicon Strip Detector, DSSD, semiconductor detector

1. INTRODUCTION

Recent soft gamma-ray observations revealed that the universe is rich of high energy phenomena of particle accelerations, associated with supernova remnants, black holes, pulsars, clusters of galaxies, gamma-ray bursts, and so on. Observations of nonthermal gamma-ray emissions is therefore important to understand the physical views of these phenomena. Diffuse unresolved gamma-ray emission is also attractive because gamma-ray emissions of annihilation or decay of dark matter particles are theoretically expected. In addition, nuclear gamma-ray lines from ^{26}Al (1.809 MeV), ^{44}Ti (1.157 MeV), ^{56}Co (0.847 MeV and 1.238 MeV), and ^{57}Co (122 keV) will give us direct information on the nucleosynthesis in the stellar interior.

However, high-sensitivity observations in the energy range of 10 keV to 20 MeV have been not available due to difficulties of imaging, detection, and background rejection. Recent developments of the hard X-ray telescope will make the sensitivity much higher below 80 keV, but the energy range of 0.1–20 MeV remains in the exploration. Since the Compton scattering is the dominant photon-matter interaction in this energy range, the Compton imaging telescope is useful. The COMPTEL onboard CGRO (Compton Gamma-Ray Observatory) is the first and sole instrument that utilizes the Compton imaging, and it was found to be very effective in the MeV gamma-ray observation. More sophisticated technique for the Compton imaging has become available, due to the improved technology of semiconductor detectors such as silicon strip detectors and CdTe (Cadmium Telluride) pixel detectors[1],[2]. Kamae et al. (1987) proposed a stack of silicon strip detectors in order to overcome the weakness of the COMPTEL[3],[4]. This idea is now extended to the concept of the Semiconductor Multiple-Compton Telescope (SMCT), which consists of multi-layer semiconductor detectors. Such a configuration has

---

Further author information: (Send correspondence to Y. Fukazawa)
Y. Fukazawa.: E-mail: fukazawa@hirax6.hepl.hiroshima-u.ac.jp, Telephone: 81 824 24 7380

advantages of good energy resolution, good angular resolution, compactness and small weight, high efficiency, effective background rejection, and so on, and is therefore very attractive for the soft gamma-ray observations.

The configuration and design of the Compton telescope depends on which energy range we observe. For the soft gamma-rays of 0.1–0.5 MeV, high energy resolution is a very important issue, because it limits the angular resolution. The Doppler broadening caused by the orbital angular momentum of electrons bound by atoms in principle limits the angular resolution, and the contribution of the energy resolution δE becomes dominant at $\delta E > 2$ keV (FWHM). We are then developing the low-noise SMCT systems with the energy resolution of $\sim$1.5 keV for the soft gamma-ray detector. The detector is a hybrid semiconductor of DSSDs and CdTe pixel detectors. The double-sided silicon strip detector (DSSD) is suitable for the scatterer because of good position resolution, good energy resolution, high scattering efficiency, and less effect of Doppler broadening. Low radio-activation in the orbit also helps us achieve the low background environment. At the photon energy of 0.1–0.5 keV, Compton scattering occurs mainly in the DSSD layers and the scattered photon is absorbed by the CdTe layers. In order to capture the photon scattered with a large angle, it is the best to surround the DSSD layers by the CdTe detectors. At higher energy, more than one scattering frequently occur, but we do not have to track more than three or more Compton scatterings to reconstruct the energy and direction of the incident photon.[3] Another possible merit of the DSSDs is that recoil electrons with > 250 keV can penetrate a DSSD of 300 μm thickness and deposit energies in two layers of DSSDs in the vacuum. In such a case, we can infer the direction of electron scattering and thus constrain the direction of the incident photon to a partial cone. Such a tighter constraint is very useful to achieve better angular resolution and more effective rejection of background. The low-noise multi-channel readout LSI is also a key technology. The detailed introduction and early demonstration have been reported by Tajima et al. (2002, 2003) and Mitani et al. (2003)[56].[7] Application for measurements of gamma-ray polarization is also attractive[8].[9] In this paper, we describe the optimization of the detector components to lmprove the energy resolution, and demonstrate the good performance of Compton imaging. The description relavant to the mission project and the performance in the combination of DSSDs and CdTe are reported in this conference proceeding[10].[11]

2. LOW NOISE DSSD SYSTEM

The low noise DSSD system consists of DSSD, RC chip, and VA32TA frontend LSI. We designed the DSSD without any other extra structures, such as bias resistors and AC coupling capacitances, so as to reduce the bad channels. Alternatively, we introduce the RC chip on which one-side silicon p-strips with polysilicon resistor and SiO_2 insulator layer are manufactured. We provide the bias voltage via polysilicon resistor and the SiO_2 AC-coupling capacitance between DSSD strips and preamplifier channels. The DSSDs and RC chips are provided by Hamamatsu Photonics, Japan, and the VA32TA is processed by IDEAS ASA, Norway.

We have produced seven types of silicon strip detectors as listed in table 1, including one-sided strip detectors for R&D. The n-strips are implanted orthogonal to the p-strips on the other side, so that we can obtain two-dimensional information of the interaction position. Since the strip capacitance is a main noise component as described later, it is worth while making it as small as possible. For that purpose, we have produced the DSSD where the strips in one direction are divided into two and they are read out from both sides. Then, the strip capacitance becomes half, while the number of readout channels is doubled. Another method to reduce the capacitance is to separate the strips as far as possible. Therefore, we procduced three types of SSDs whose strip gap is different among them.

We produced RC chips with two different bias resistances and three different coupling capacitances. The bias resistance and coupling capacitance of RC chips are typically 1.0–6.0 GΩ and 22–110 pF, respectively. Since the RC chip is small, an additional capacitance noise is not significant. The VA32TA is 32-channel low-noise MOS amplifier that includes preamplifier, shaper, sample/hold, analog multiplexer, and discriminator, and processed by the 0.35 μm AMS technology to increase the radiation hardness.[12] The size of the frontend MOSFET for the preamplifier is optimized for the low-noise operation. Majority selector circuits for the register to ensure the tolerance against the Single-Event Upset (SEU) is implemented for space applications. The electric power consumption is 6.3 mW/channel, and the pad pitch is 100 μm. More detailed explanation of the VA32TA is described in Tajima et al. 2002.[5]

3. BASIC PROPERTIES OF SILICON STRIP DETECTORS

At first, we measured the leakage current, interstrip capacitance, and body capacitance of p-strips for each type of DSSDs and RC chips, in order to evaluate the noise performance.[13] In table 1, the results are summarized. The measurements were performed at 20 °C, and we listed the leak currents and the capacitances measured at 100 V for DSSDs and 30 V for RC chips.

Overall, the interstrip and body capacitance is around 2–4 pF per channel. As described after, this is enough to achieve the energy resolution of ~1.5 keV. As seen from the comparison between the SSD (a) and (b), the capacitance becomes certainly half when the strip is divided into two. The SSDs with different strip gaps of 100, 130, and 160 μm, [DSSD (f), (g), and (h)], certainly show a different interstrip capacitance. but the difference is small by at most 20%, not so significant to affect the noise performance.

The leakage cuttent of all the DSSDs is at most 0.1–0.5 nA per channel, indicating that the noise relavant to the leakage current can be negligible at 0°C. Generally, the leakage current is larger for the wider strip gap, due to stronger distortion of the electric field. However, since the leakage current is not so different among the DSSD (f), (g), and (h), the strip gap of 160 μm is accepted. The capacitance and leakage current of the RC chip are at most 1.5 pF and 0.1 nA per channel, respectively, and thus the contribution to the noise performance is small.

In summary, the trial products of the DSSDs exhibited as good characteristics as we expected, and therefore we next investigated them as X-ray detectors for the Compton camera.

Table 1. Summary of the DSSDs and their properties.

Type	Strip parameters				Basic properties per p-strip channel		
	pitch	gap	length (cm)	thickness	Leak-I^a (nA)	Body-C^b	Inter-C^c
(a)SSD-A	200	160	3.8	400	0.12	2.1	2.0
(b)SSD-B	300	260	1.7	400	0.03–0.08	1.3	0.9
(c)DSSD400	400	100	2.56	300	0.47	3.4	2.6
(d)DSSD800	800	100	2.56	300	0.32	6.9	2.6
(e)DSSD8002	800	100	1.27	300	0.15	3.5	1.1
(f)SSD100	400	100	2.56	300	0.36	6.3	–
(g)SSD130	400	130	2.56	300	0.41	5.7	–
(h)SSD160	400	160	2.56	300	0.49	5.2	–
RC chip 1	200	–	–	300	0.03	0.07	1.2
RC chip 2	400	–	–	300	0.09	0.15	1.3
RC chip 3	800	–	–	300	0.09	0.31	1.5

a: current, b: body capacitance, c: interstrip capacitance
The unit is μm for strip pitch, gap, and thickness, and pF for capacitance.
Measurements were performed at 20 °C, with the bias voltage of 100 V for DSSDs and 30 V for RC chips.
The bias resistance and coupling capacitance of RC Chips are typically 1.0–6.0 GΩ and
22–110 pF, respectively.

4. SETUP AND GAMMA-RAY RESPONSE

We connected the DSSD with the frontend LSI VA32TA to readout the strip channels (figure 1). Here we prepared two DSSD+VA32TA sets, for which we use DSSDs (c) with the strip pitch of 400 μm. Since n-strips intrinsically have a larger capacitance due to the Ohmic-junction of p$^+$ and n$^+$, we use them only for position measurements and mainly p-strips for pulse-height measurements. Taking into account that the RC chip would introduce some noise, we couple p-strips directly (DC-coupling) and n-strips via two RC chips (AC-coupling) with VA32TA. We then set the voltage difference between two sides to 100 V for DSSDs, and to 20 V and 50 V for two RC chips, by supplying the voltage as shown in figure 2. The reason why we use two RC chips is that the

voltage tolerance of the coupling capacitance is low. Here we used two types of RC chips, 1 and 2, for n-strips on two DSSDs. We also supplied the same voltage as strips to the guard rings. 64 strips of each P or N side are readout by two VA32TA chips, which is set up by the VA-DAQ provided by IDEAS, through the LabVIEW software. The set-up parameters for the VA32TA are optimized as described in §5.
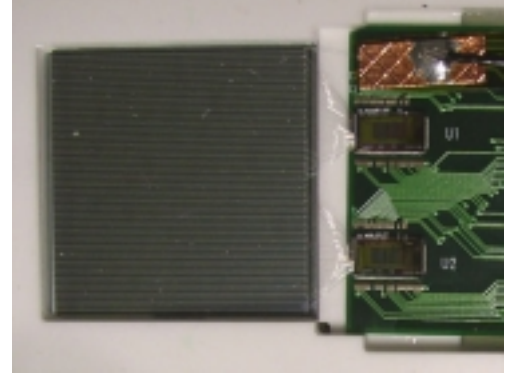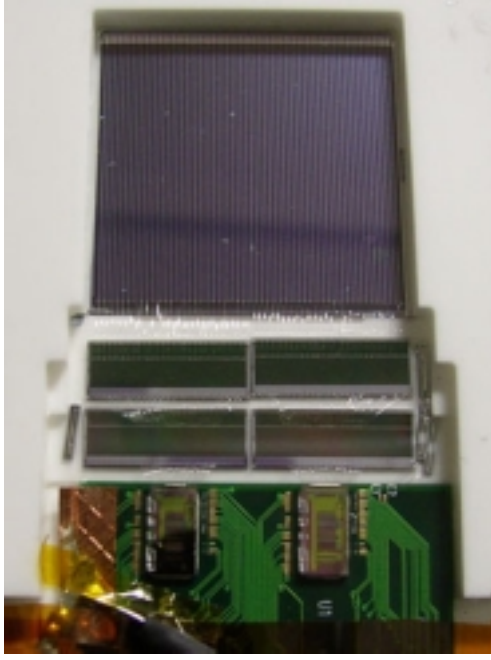

Figure 1. Setup of DSSD, RC chip, and VA32TA.

We then measured the gamma-ray response of the DSSDs at -10 °C, by irradiating various radio-isotopes. We calculated the pedestal of each channel by averaging the pulse-height for each data set of $\sim$ 3000 events with no hits in the corresponding channel. Also we estimated the common mode noise of each event by averaging the pulse-height over channels with no hits. The root-mean-square of the common mode noise is typically 0.5–0.6 keV (Si). The pedestal and common mode noise are subtracted from the ADC channel. The linearity function is obtained by utilizing the six gamma-ray lines of 13.927, 17.506, 20.895, and 59.54 keV from ^{241}Am and 14.4 and 122.06 keV from ^{57}Co. Figure 3 left shows the residual of the ADC channel of each photo-peak line when the relation between the gamma-ray energy and the ADC channel is fitted with the linear function. The residual distributed over -0.6 to 0.6 keV. Such a significantly large residual indicates that the relation between the gamma-ray energy and the ADC channel is not linear. The large difference of $\sim$0.5 keV leads to incorrect reconstruction
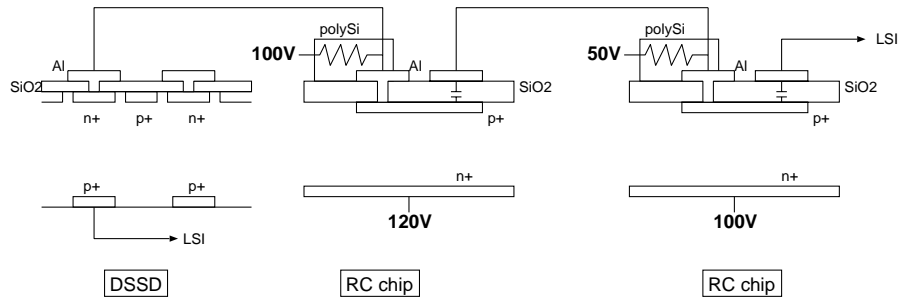

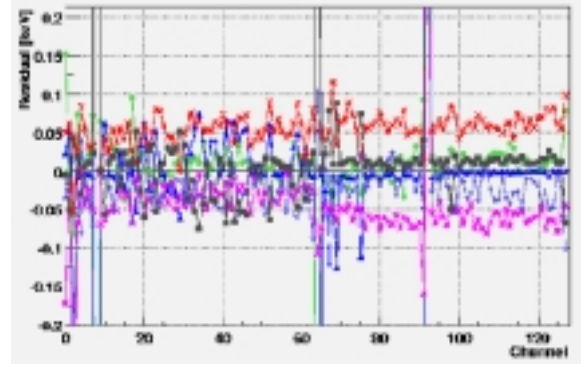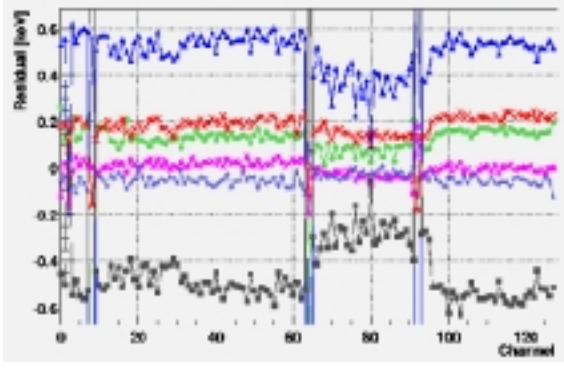**Figure 2.** Setup of bias voltage supply.

Figure 3. Redidual in unit of keV when we fit the relation between the gamma-ray energy and the ADC channel for linear function (left) and exponential function (right).
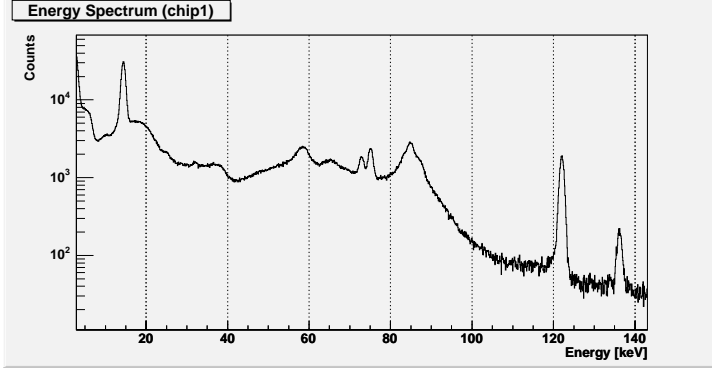

Figure 4. Pulse-height spectrum of DSSD systems for ^{57}Co irradiation. The spectrum was summed up over p-strips on one DSSD.

in the Compton scattering and makes the angular resolution worse. When we introduce the emperical formula of $E = a - b\exp{(-\text{CH}/c)}$, where E is a gamma-ray energy in keV, CH is an ADC channel, and a, b, c are free parameters, the residual becomes as small as < 0.1 keV, as shown figure 3 right.[14] In the following, we utilize this formula in converting the ADC channel to energy. We also confirmed that the gain is stable, in such a way that the pulse-height channel of photo-peaks does not vary in measurement by measurement within <1 %.

The pulse-height ratio of n-strips to p-strips for the same gamma-ray energy is 0.57 for one DSSD and 0.48 for another. This is due to the charge loss caused by the capacitance of DSSDs and RC chips, which cannot be neglected in comparison with the coupling capacitance. Here the difference of pulse-height ratio between two DSSDs is explained by the difference of coupling capacitance. The charge collection efficiency ε is expressed as $\varepsilon = \frac{C_{\text{couple}}}{C_{\text{couple}}+C_{\text{DSSD}}+C_{\text{RC}}}$, where C_{couple}, C_{DSSD}, and C_{RC} are capacitances of coupling condensers, DSSDs, and RC chips. In this measurement, we used two RC chips for one DSSD and thus the C_{couple} becomes half. Inserting the values listed in table 1, ε is calculated to be 0.73 and 0.57 for the coupling capacitance of 44 and 22 pF per one RC chip. These values are consistent with the measurement one, but somewhat larger possibly due to the stray capacity.

Figure 4 shows the pulse-height spectrum of ^{57}Co, obtained for all the p-strips on one DSSD. The photopeaks of 14, 122, and 135 keV are seen in the spectra, together with the back-scatter line structure around ~ 85 keV. We also see the clear separation of the Pb $K\alpha_1$ and $K\alpha_2$ (74.97 and 72.80 keV) from the ambient Pb shield. The energy resolution (FWHM) of one DSSD is 1.13 ± 0.02 keV and 1.32 ± 0.03 keV for the peak of 14 keV and 122 keV, and the noise estimated as a root-mean-square of pulse height for strips whose signal is less than the threshold is 1.02 ± 0.01 keV. The expected noise performance of the VA32TA is $(0.37 + 0.16 \times C_d)/\sqrt{\tau}$ (FWHM, keV) where C_d is the load capacitance in pF and τ is the shaping time in μs, and becomes 0.77 keV for $C_d = 6.0$ pF and $\tau = 3$ μs. The shot and thermal noise are estimated to be 0.38 keV and 0.36 keV, respectively, by
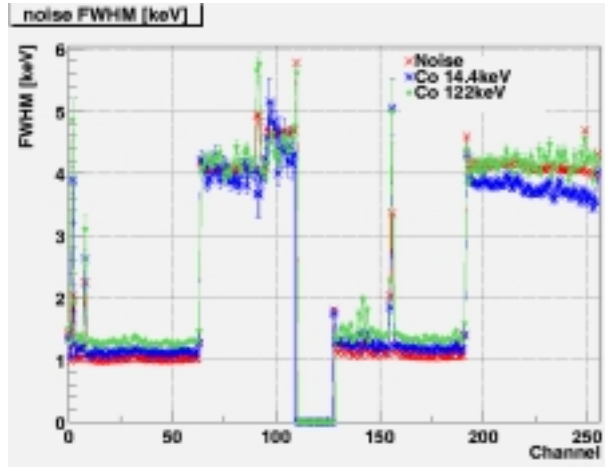
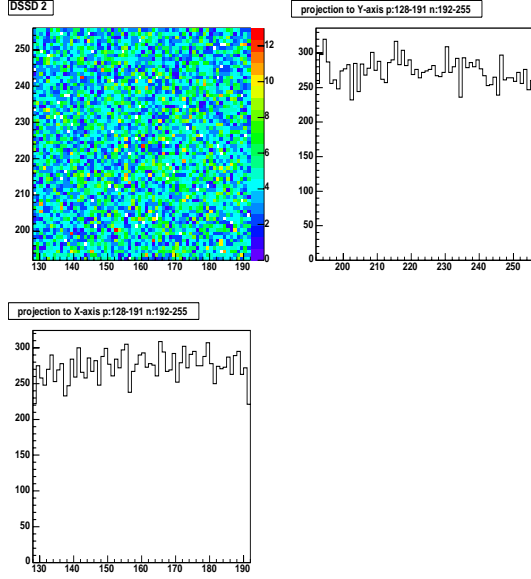**Figure 5.** Energy resolution of 122 keV for each channel.

Figure 6. The left-top panel is the two-dimensional distribution of detected gamma-rays (122 keV) in the DSSD. The right-top and left-bottom are the one-dimensinal count distribution for n and p strips, respectively.
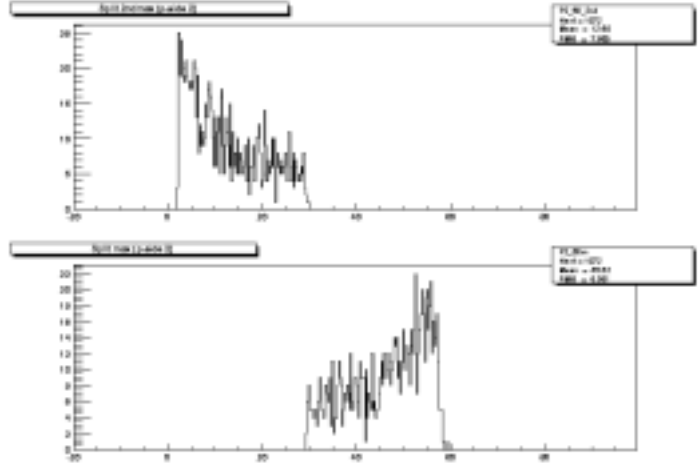

Figure 7. Spectra of the E_1 (top) and E_2 (bottom) for split events for 59.5 keV gamma-rays. The horizontal axis is in unit of keV. See text in detail.

assuming that the leakage current becomes small by a factor of 2 as the temperature decreases by 7 degree. Then the total expected noise is 0.93 keV, and it becomes 1.03 keV when including the poisson noise for the 122 keV gamma-ray. These values are better than the experimental values, partly due to that the experimental values may suffer the unrecognized electric noise.

Figure 6 shows the two-dimensional distribution of detected gamma-rays (122 keV) in the DSSD, together with the one-dimensinal count distribution for p and n strips. Here we chose the events whose signal is within 4σ around 122 keV. Although somewhat more photons are detected around the center region due to the incomplete flatness of gamma-ray irradiation, the count distribution in each strip almost follows the Poisson distribution.

Since the 122 keV gamma-ray is detected almost uniformly along the depth direction of the DSSD, the flatness of count distribution indicates that the depletion layer developed uniformly and signal charge is efficiently collected everywhere.

Next we investigated the frequency of split events, in which the signal charge is split into and detected by two strips. We considered it as a split event that the neighboring p-strips, together with one n-strip or two neighboring n-strips, give the signal above the threshold, and the sum of their p-strip signals is within the 4σ of the photo-peak line. We here denote the signal of two p-strips as E_1 and E_2 ($E_2 > E_1$). Figure 7 shows the spectra of the E_1 (top) and E_2 (bottom) for split events in the case of 59.5 keV gamma-ray irradiation. It can be seen that the pulse height channel distributes with the tail. The frequency of split events is $7.6 \pm 0.2\%$, $3.4 \pm 0.1\%$, and $0.026 \pm 0.003\%$ for 122, 59.5, and 17.6 keV, respectively. The probability that such an event is caused by the Compton scattering is much lower. We also confirmed that the split event occurs with almost the same frequency for all the strips. As a result, the splitting of signal charge is not so significant for soft gamma-ray detection.

5. OPTIMIZATION AND NOISE PERFORMANCE OF THE DSSD AND THE FRONTEND CIRCUIT

The VA32TA has several set-up parameters, such as bias currents and voltages to the FET, on/off flags of readout channels, and some selection flags for operation. These information are sent to the VA32TA as digital bits, and the actual bias voltage and current are produced by internal DACs in the VA32TA. We investigated the noise performance for various values of bias voltage and current in order to find the optimized set-up values.

We measured the parameter dependence of the energy resolution of the DSSD and VA32TA system, by irradiating the gamma-ray 122 keV of the radio-isotope ^{57}Co. Among VA parameters, the most sensitive to the noise performance are the bias current for the preamplifiers (prebias) and for controlling the slow shaper feedback resistance (Ifss). The latter parameter determines the shaping time. In figure 8, we show the parameter dependence of the strip-averaged energy resolution measured at 0 °C. For the bias current to the preamplifiers, the energy resolution varies in the range of 1.4–1.6 keV, and the best is given at 200–250 μA. The Ifss gives a larger variation of the energy resolution, which becomes the best around 40–60 nA, corresponding to the shaping time of ~3 μs. The larger Ifss gives the shorter shaping time, and thus the capacitance noise becomes dominant, while the smaller Ifss (longer shaping time) introduces signal filtering loss by the shaping amp. Note that the shot noise is negligible at 0 °C.

The pulse-height and energy resolution are also dependent on the temperature. This dependence is attributed to the VA32TA. Figure 9 shows the temperature dependences of the above quantities averaged in p-strips. The pulse-height becomes somewhat larger with the coefficient of 0.4%/°C. This coefficient becomes larger for the smaller bias current of preamplifiers. The energy resolution becomes better at the lower temperature, maybe due to the noise performance of preamplifiers.

6. COMPTON IMAGING

Combining the two DSSD systems, we performed the Compton imaging to confirm the angular resolution.[14] We placed the two DSSDs in parallel with the separation of 6.7 mm, and irradiated the gamma-ray source ^{57}Co at 56.4 mm away from the DSSD. The gamma-rays are collimated by the ϕ2 mm Pb hole with 2mmt. The experiment was performed at -10 °C. In figure 10, we show the scatter-plot of E_1 and E_2, which are defined as in §4. We can see the two lines running diagonally, corresponding to the Compton-scattering and split events for 122 keV and 136 keV.

We selected the Compton-scattering events as follows. We first choose the events in which the enery deposition with > 10 keV occurs in at least two p-strips ($E_2 > E_1 > 10$ keV). Based on the Compton kinematics for 122 keV gamma-rays, we exclude the events with $E_1 > 45$ keV. Furthermore, in the case that the two p-strips neighbor each other, we consider it as a split event and exclude it. We also exclude the events whose signal at the n-strip which is on the same DSSD with the hit p-strips is different from that of p-strips by more than 8 keV. We then accepted the events whose $E_1 + E_2$ is within the energy resolution of $2\sigma \sim 1.3$ keV from 122 keV. 33% of all the Compton-scattering events is the ones where the hit occurs in two DSSDs, and 70% of such events are
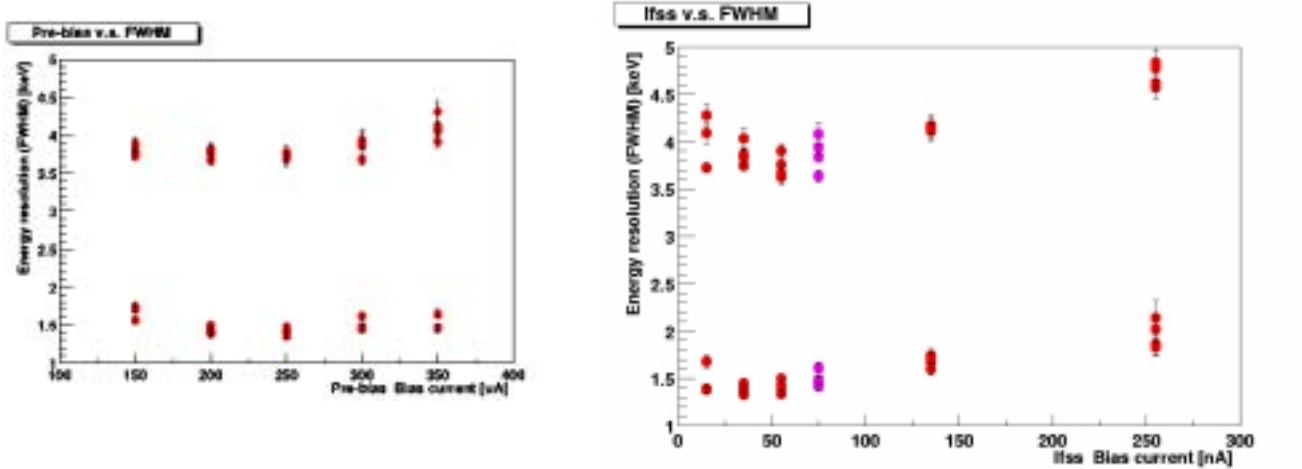
Figure 8. Strip-averaged energy resolution for 122 keV against the bias current to the preamplifiers (left) and Ifss (right). The data around 1.5 keV and 4 keV are those of p- and n-strips, respectively. Both strips are readout with 4 VA32TA chips, and thus there are 4 data points for each strip.
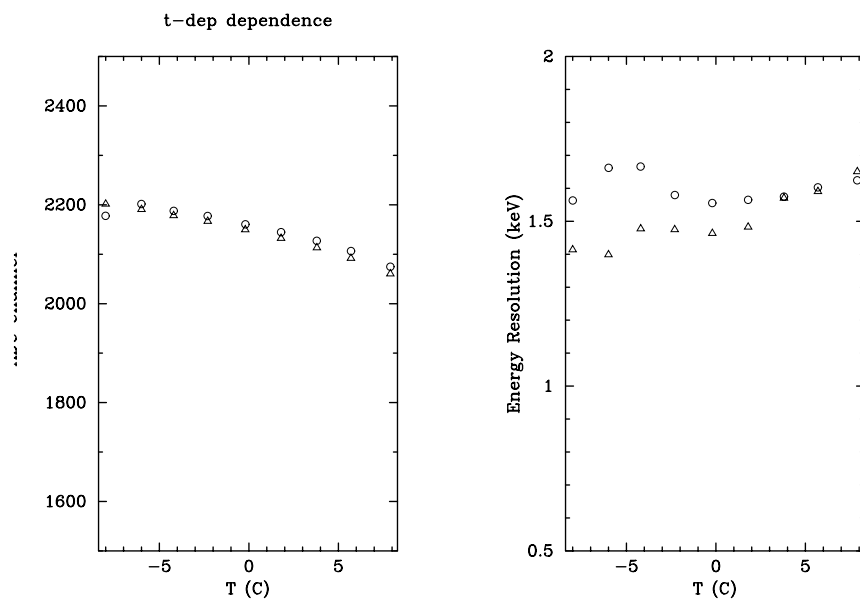

Figure 9. Strip-averaged pulse height (left) and energy resolution (right) for 122 keV against the temperature.
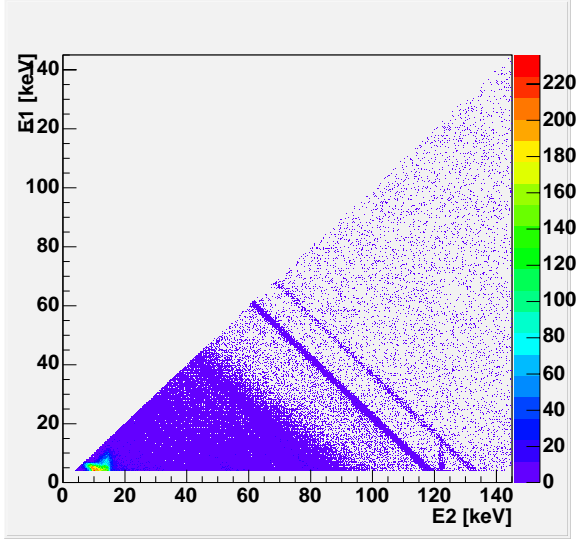
Figure 10. The scatter-plot of E_1 and E_2.

Figure 11. The definition of angles for reconstruction.

the forward scattering events. The $E_1 + E_2$ follows the gaussian with the FWHM of 1.8 keV, reasonable when considering that both E_1 and E_2 follow the gaussian with the FWHM of 1.3 keV.

After selecting the Compton events, we reconstructed the incident direction of gamma-rays (figure 11). The order of hits in the Compton scattering of the 122 keV gamma-ray is explicitly determined; the hit with the lower energy deposition occurs first. The axis v of the Compton cone is determined by the vector pointing from the second hit position p_2 to the first p_1 ($v = p_1 - p_2$). The scattering angle θ_{sc} is calculated by the deposite energy of both hits as $\cos\theta_{\mathrm{sc}} = 1 + \frac{m_e c^2}{E_1 + E_2} - \frac{m_e c^2}{E_2}$. Then we obtained the reconstructed image of the gamma-ray source by intersecting the Compton cone around the axis v with the arbitrary plane. The origin of the Compton cone is p_1. Here we set the plane at the same distance of the radio isotope of 122 keV. Figure 12 left shows the reconstructed image of gamma-ray sources, in which the source clearly appears. For evaluating the angular resolution, we defined the angle of the vector v against the vector $u = p_0 - p_1$ as θ_{geo}, where p_0 is the center position of the radio isotope. The angle difference $\delta\theta = \theta_{\mathrm{sc}} - \theta_{\mathrm{geo}}$ should be 0 if the reconstruction is complete and the gamma-rays are emitting from the ideal point source. We plot the distribution of $\delta\theta$ in figure 12 right. The FWHM of the angle distribution is ~ 8 degree.

In order to check whether the FWHM of the above angle distribution is reasonable for the setup of this experiment, we performed the simulation with the package Geant 4.5.1 by constructing the metarial geometry of the experimental setup, injecting the gamma-ray, and reconstructing the image in the same way as the real data. The standard process in the Geant 4 does not include the effect of Doppler broadening, and we replace the original process of the Low-Energy Compton scattering by the G4LECS ver 1.03 provided by R. M. Kippen.[15] The Doppler broadening is considered in the G4LECS in such a way that the treatment of Compton scattering accounts for bound electron momentum on a shell-by-shell basis using evaluated data read from tables. As a result, we obtained allmost the same FWHM as the experimental one. This FWHM value mainly reflects the four effects; (a) Doppler broadening, (b) energy resolution, (c) position resolution of the DSSD, and (d) finite size of the gamma-ray source. We simulated by including these effects step-by-step, to investigate how each of these effects makes the FWHM large. Here we set the energy resolution to 1.3 keV. At first, the distribution for only (a), the limit by the Dopper broadening, is found to be expressed by two gaussins with the sigma of 1.30 degree and 6.18 degree. The distribution of other cases is thought to be modeled by smoothing this formula with the gaussian. After including the effect (d), the smoothing parameter σ is 1.44±0.25 degree, indicating that the effect of finite size of gamma-ray sources is small. Then it becomes larger as 1.94 ± 0.37 degree and 1.67 ± 0.65 degree for the case (a)+(b)+(d) and (a)+(b)+(c)+(d), respectively. The experimental data give the $\sigma = 2.36 \pm 0.56$ degree, and we confirmed that the experimental is reasonable. In the multi-layer configuration of the Compton
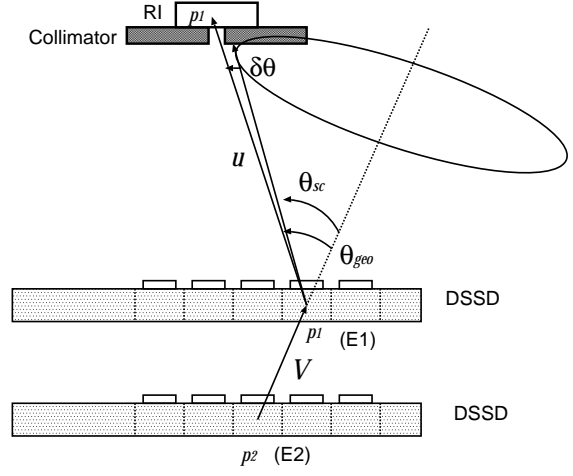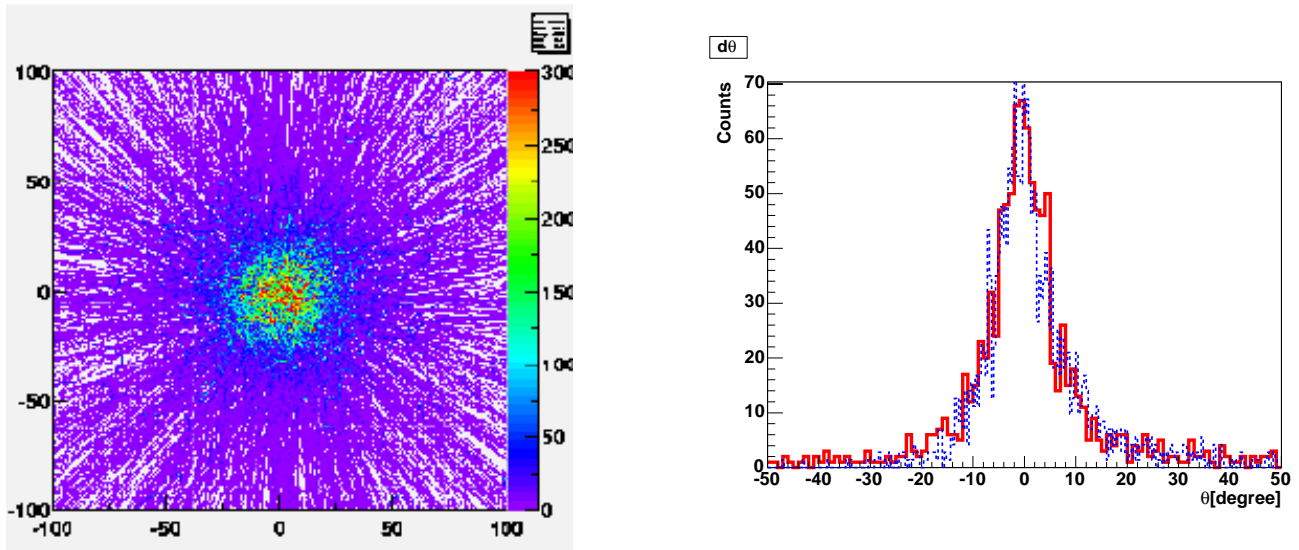
Figure 12. Left panel is a reconstructed image for 122 keV gamma-ray. Right is the histogram of $\delta\theta$. The solid and dashed line represent the experimental data and simulation, respectively. See text in detail.

camera, most of hits occur in a larger separation, and thus the effect (c) becomes smaller. Therefore, the angular resolution of DSSD multi-layer Compton camera corresponds to the case of (a)+(b), $\sigma = 0.80 \pm 0.33$ degree. It can be seen that the effect (b) is smaller than that of (a), and it can be said that the noise performance of the DSSD system satisfies the goal that the contribution of energy resolution to the angular resolution is less than that of Doppler broadening.

7. CONCLUSION

We fabricated the prototype DSSD and VA32TA frontend LSI for the low-noise Compton camera system. The energy resolution for 122 keV gamma-ray is obtained to be 1.3 keV (FWHM) for the p-strip DC-readout configuration. This is good enough to approach the Doppler-broadeing limit of angular resolution of the Compton camera. Also we constructed the two-layer DSSD Compton camera and confirmed that the gamma-ray image is reconstuted with the angular resolution in compatible with that we predicted.

We are now testing the next prototype DSSD whose size is 4×4 cm^2 with a strip pitch of 400μm and a thickness of 300 μm. The size of 4×4 cm^2 with a thickness of 500 μm is the largest processed for 4-inch wafers, and it will be the goal. As described in this paper, the noise is dominated by the load capacitance and the frontend amplifier noise. Therefore, it is worth while trying the reduction of DSSD capacitance by the readout from both sides of strips divided into two. Also, we have a plan to further optimize the frontent MOS-FET and lower the electric power of LSI. Furthermore, it is important to establish how to stack the multi-layer DSSD and CdTe, together with the frontend LSI, in the compact size.

REFERENCES

1. T. Takahashi, K. Nakazawa, T. Kamae, H. Tajima, Y. Fukazawa, M. Nomachi, and M. Kokubun, "High Resolution CdTe Detector and its Application to the Next Generation Multi Compton Telescope," in *X-ray and Gamma-ray Telescopes and Instruments for Astronomy, Proc. SPIE* **4851**, p. 1228, 2002.

2. T. Takahashi, K. Makishima, Y. Fukazawa, M. Kokubun, K. Nakazawa, M. Nomachi, H. Tajima, M. Tashiro, and Y. Terada, "Hard X-ray and Gamma-Ray Detectors for the NEXT mission," *New Astronomy Reviews* **48**, p. 309, 2004.

3. T. Kamae, R. Enomoto, and N. Hanada, "A new method to measure energy, direction, and polarization of gamma rays," *Nucl. Inst. and Meth. A* **260**, p. 254, 1987.

4. T. Kamae, N. Hanada, and R. Enomoto, "Prototype design of multiple Compton gamma-ray camera," *IEEE Trans. Nucl. Sci.* **35**, p. 352, 1988.

5. H. Tajima, T. Kamae, S. Uno, T. Nakamoto, Y. Fukazawa, T. Mitani, T. Takahashi, K. Nakazawa, Y. Okada, and M. Nomachi, "Low Noise Double-Sided Silicon Strip Detector for Multiple-Compton Gamma-ray Telescope," in *X-ray and Gamma-ray Telescopes and Instruments for Astronomy*, *Proc. SPIE* **4851**, p. 875, 2002.

6. H. Tajima, T. Nakamoto, T. Tanaka, S. Uno, T. Mitani, E. Silva, Y. Fukazawa, T. Kamae, G. Madejski, D. Marlow, K. Nakazawa, M. Nomachi, Y. Okada, and T. Takahashi, "Performance of a Low Noise Front-end ASIC for Si/Cdte Detectors in Compton Gamma-ray Telescope," *IEEE Trans. Nucl. Sci.* **in press**, 2004.

7. T. Mitani *et al.*, "Performance of Compton Camera using High Resolution Si/CdTe detectors – Si/CdTe Compton camera as a polarimeter –," *IEEE Trans. Nucl. Sci.* **in press**, 2004.

8. H. Tajima, "Gamma-ray polarimetry," *Nucl. Instrum. Methods A* **511**, p. 287, 2003.

9. H. Tajima *et al.*, "Gamma-ray Polarimetry with Compton Telescope," *Proc. SPIE*, 2004.

10. T. Takahashi, "Wide-band x-ray imager (WXI) and soft gamma-ray detector (SGD) for the NEXT mission," in *UV and Gamma-Ray Space Telescope Systems*, *Proc. SPIE*, 2004.

11. T. Tanaka, T. Mitani, K. Nakazawa, K. Oonuki, G. Sato, T. Takahashi, K. Tamura, S. Watanabe, H. Nakamura, M. Nomachi, T. Nakamoto, and Y. Fukazawa, "Development of Si/CdTe semiconductor Compton Telescope," *Proc. SPIE*, 2004.

12. M. Yokoyama *et al.*, "Radiation hardness of VA1 with sub-micron process technology," *IEEE Trans. Nucl. Sci.* **48**, p. 440, 2001.

13. S. Uno, "Development of low-noise double-sided silicon strip detector for cosmic gamma-rays," *Master Thesis in Japanese i(Hiroshima University)* , 2003.

14. T. Nakamoto, "Development of multi-layer silicon strip detector and BGO/Photodiode for soft gamma-ray Compton camera," *Master Thesis in Japanese (Hiroshima University)* , 2004.

15. R. M. Kippen, "G4LECS," in *http://nis-www.lanl.gov/~mkippen/actsim/g4lecs/*, 2003.